On the nature of OH-stretching vibrations in hydrogen-bonded chains: Pump frequency dependent vibrational lifetime

ARTICLE *in* PHYSICAL CHEMISTRY CHEMICAL PHYSICS · MARCH 2011

Impact Factor: 4.49 · DOI: 10.1039/c0cp02143a · Source: PubMed

4 AUTHORS, INCLUDING:

Stephan Knop
University of Bonn
12 PUBLICATIONS **53** CITATIONS
SEE PROFILE

Thomas La Cour Jansen
University of Groningen
78 PUBLICATIONS **1,720** CITATIONS
SEE PROFILE

Peter Vöhringer
University of Bonn
108 PUBLICATIONS **1,849** CITATIONS
SEE PROFILE

PCCP

View Online
Dynamic Article Links

Cite this: *Phys. Chem. Chem. Phys.*, 2011, **13**, 4641–4650

www.rsc.org/pccp

PAPER

On the nature of OH-stretching vibrations in hydrogen-bonded chains: Pump frequency dependent vibrational lifetime

Stephan Knop,[a] Thomas La Cour Jansen,[b] Jörg Lindner[a] and Peter Vöhringer*[a]

Received 13th October 2010, Accepted 22nd December 2010
DOI: 10.1039/c0cp02143a

Two-dimensional infrared spectroscopy was carried out on stereoselectively synthesized polyalcohols. Depending upon the stereochemical orientation of their hydroxyl groups, the polyols can either feature linear chains of hydrogen bonds that are stable for extended periods of time or they can display ultrafast dynamics of hydrogen-bond breakage and formation. In the former case, the OH-stretching vibrations and their transition dipoles are substantially coupled, hence prior to vibrational relaxation, the initial OH-stretching excitation is rapidly redistributed among the set of hydroxyl-groups constituting the hydrogen-bonded chain. This redistribution is responsible for an ultrafast loss of memory regarding the frequency of initial excitation and as a result, a pump-frequency independent vibrational lifetime is observed. In contrast, in the latter case, the coupling of the OH-groups and their transition dipoles is much weaker. Therefore, the OH-stretching excitation remains localized on the initially excited oscillator for the time scale of vibrational energy relaxation. As a result inhomogeneous relaxation dynamics with a pump-frequency-dependent lifetime are observed.

Introduction

Hydrogen bonding (H-bonding) is a ubiquitous phenomenon in nature. It is a key element in defining the three-dimensional structure, the dynamics, and the function of chemical and biochemical molecular systems.[1,2] The interaction energies involved in the formation of intra and intermolecular hydrogen bonded contacts are rather diverse, ranging between a few kJ per mol for weak H-bonds (*e.g.* N–H$\cdots\pi$ systems) to a few tens of kJ mol^{-1} for very strong H-bonds (*e.g.* the symmetrical hydrogen bifluoride anion). Thus, H-bonds can be comparable in strength to covalent bonds or they can be as weak as simple van der Waals-interactions.[2]

Most intriguingly, in systems exhibiting some degree of spatial periodicity involving hydrogen donor and acceptor moieties, H-bonding can become a highly cooperative phenomenon leading to the formation of entire networks of hydrogen-bonds. The most prominent examples of which are the H-bond networks of associated liquids and solids such as water and ice. Depending upon the strength of the H-bond, the thermally induced structural fluctuations within these networks can occur over a wide spectrum of time and length scales and consequently, the study of the spatio-temporal evolution of hydrogen-bonded systems by physico-chemical means is at the center of contemporary condensed phase research.[1,2]

In particular, various variants of femtosecond time-resolved vibrational spectroscopy have proven tremendously helpful in revealing ultrafast molecular dynamical processes in H-bonded liquids.[3,4] For example, mid-infrared (mid-IR) pump–probe and multidimensional spectroscopies have elucidated vibrational energy relaxation[5–12] and vibrational spectral diffusion[13–17] in the hydroxyl (OH) stretching spectral region of liquid water. Unfortunately, the structure and the molecular dynamics of naturally occurring liquid networks are usually highly random. Their complex stochastic character, in both space and time, precludes a systematic study of size effects related to the collective properties of the spectroscopic observables and of their underlying vibrational degrees of freedom.

In an effort to address the quantum-mechanical nature of the OH stretching modes as well as to explore the intra and intermolecular couplings of hydroxyl vibrators engaged in cooperative H-bonding, we have recently introduced stereo-selectively synthesized polyalcohols as low-dimensional model systems for the vibrational spectroscopy of naturally occurring random hydrogen bond networks.[18] Besides reducing the three-dimensional extension of the network to a simple quasi-linear chain, these species facilitate a full control of the size of the resultant hydrogen-bonded array *via* the sheer number of hydroxyl groups attached by the chemical synthesis to a conformationally controlled saturated hydrocarbon backbone.

[a] *Lehrstuhl für Molekulare Physikalische Chemie, Institut für Physikalische und Theoretische Chemie, Rheinische Friedrich-Wilhelms-Universität, Wegelerstraße 12, 53115 Bonn, Germany. E-mail: p.voehringer@uni-bonn.de*
[b] *Centre for Theoretical Physics and Zernike Institute for Advanced Materials, University of Groningen, Nijenborgh 4, 9747 AG Groningen, The Netherlands*

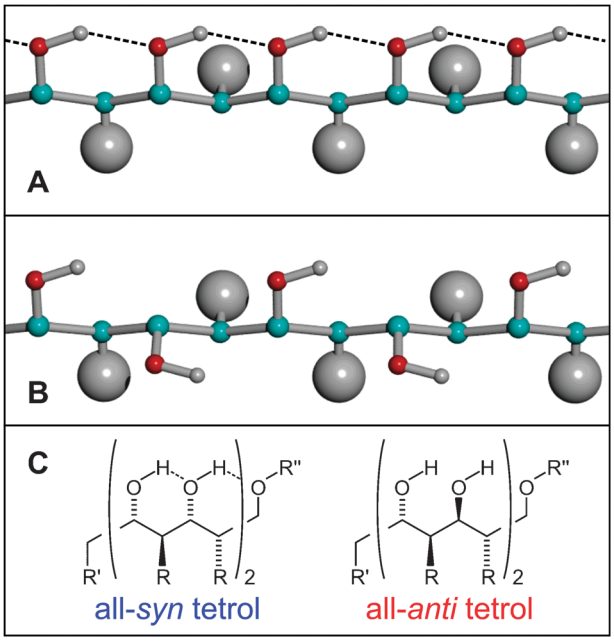

Fig. 1 Schematic structure of an all-*syn* polyol (A) and an all-*anti* polyol (B). The hydrocarbon backbone (H-atoms not shown) is conformationally controlled through the steric repulsion between the bulky substituents (large spheres, here methyl groups) occupying the 1,3-*anti* directions. Depending upon the stereochemical orientation of the hydroxyls an extended hydrogen bonded network (dashed) may or may not form. The chemical structures of the systems studied here are shown in panel C.

The basic features of these polyols are sketched in Fig. 1. They can be regarded as long-chain alkanes carrying an alternating hydroxyl-methyl substitution pattern. A stereoregular 1,3-*anti* alkylation intends to stabilize an extended all-*trans* conformation of the hydrocarbon. Introducing the hydroxyls in a 1,3-*syn* fashion is expected to favor the formation of an extended hydrogen-bond chain-like network while a 1,3-*anti* hydroxylation should avoid intramolecular H-bonded contacts altogether or at least weaken them to a considerable extent. These ideas based on the work by Paterson and co-workers[19] have been supported by detailed quantum chemical calculations of the molecular structure at 0 K using density functional theory (DFT) as well as by Langevin simulations of the molecular dynamics at finite temperature in the presence of a condensed phase environment.[18]

Whereas we focused previously on the vibrational dynamics observed through conventional mid-IR pump–probe spectroscopy with broadband-pumping of the apparent OH-stretching mode, the emphasis is here on the population dynamics initiated by excitation pulses of varying center frequency. The work presented here provides direct evidence from a dynamical variable—the pump frequency-dependent vibrational lifetime, $\tau(\nu_{pump})$—for a very rapid initial redistribution of the OH-stretching excitation among the collection of coupled hydroxyl groups in the case where an extended network of hydrogen bonds is facilitated (*i.e.* all-*syn* tetrol). In contrast, the OH-stretching excitation remains predominantly localized on the initially excited hydroxyl groups when such a network formation is stereochemically hindered (all-*anti* tetrol). The results reported here have important implications for the mechanism of vibrational energy flow in hydrogen-bonded liquids.

Experimental

Femtosecond mid-infrared pump–probe experiments were performed in the dynamic hole burning setup introduced by Hamm and Hochstrasser[20] using a laser system that consisted of a commercial femtosecond front-end (Clark-MXR, CPA 2001) for synchronously pumping two optical parametric amplifiers (OPA). The combined signal and idler output of each OPA was mixed in $AgGaS_2$ for phase-matched type-I difference frequency generation (DFG) of mid-infrared light. One of the OPA/DFG devices served as the pump source while the other provided the probe light. An etalon was used to spectrally shape the excitation pulses into a Lorentzian profile with a narrow width of 25 cm^{-1} (FWHM). Pump and probe pulses were focused into the sample using a 45° off axis parabolic Au mirror (OAP) with an effective focal length of 100 mm. An identical OAP was used to collimate the beams after the sample and to image the probe pulse onto the entrance slit of a 0.2 m monochromator whose exit slit was replaced by a 2 × 32 element HgCdTe array detector for probe frequency-resolved referenced detection. Spectra were recorded with the relative pump–probe polarization set to the magic angle. IR absorption spectra were recorded with a commercial FTIR spectrometer (Nicolet 5700, Thermo Fisher) at a resolution of 2 cm^{-1}. The samples consisted of solutions of the polyols in deuterated chloroform and were contained in static cells equipped with CaF_2-windows that were separated by 2 mm spacers. A rotation of the sample cell during data acquisition to avoid thermal effects and to replenish the sample after the actinic event does not modify the pump–probe signals. The time-resolution after shaping the excitation pulses by the etalon was determined to be 300 fs (FWHM) by recording the pump–probe response of a 100 μm thick Germanium substrate.

The concentration was adjusted to 6 mM in $CDCl_3$, which resulted in a linear optical density of the sample of 0.25 at a thickness of 2 mm with negligible poly-alcohol aggregation (see below). Although the paper reports only data on (2*R*,3*S*,4*S*,5*S*,6*R*,7*S*,8*R*,9*R*)-1-benzyloxy-2,4,6,8-tetramethyl-undecane-3,5,7,9-tetrol (all-*syn* tetrol) and on (2*R*,3*R*,-4*S*,5*S*,6*R*,7*R*,8*R*,9*R*)-1-benzyloxy-2,4,6,8-tetramethylundecane-3,5,7,9-tetrol (all-*anti* tetrol), complementary investigations on shorter and longer species have also been carried out. They are in full agreement and support the general significance of the reported results and conclusions obtained on the tetrols. The diastereomeric polyols were synthesized according to the protocols outlined in detail in ref. 19 and 21. Their purities were checked by nuclear magnetic resonance and the results fully confirm the superb diastereoselectivity of the iterative boron-assisted aldol condensation developed by Scott and Paterson.

Details related to quantum chemical calculations on the polyols were already presented in ref. 18. Briefly, density functional theory was applied using the ORCA program package, the Becke-Perdue functional, BP86, and Ahlrich's triple-ζ valence basis set, TZVPP, including the Coulomb

fitting basis, TZV/J, as required for invoking the efficient resolution-of-identity approximation. Geometry optimizations were performed in redundant internal coordinates using analytical gradients whose double-sided numerical differentiation was required for a normal modes analysis of the systems.

Results and discussion

A mid-IR absorption spectrum in the CH- and OH-stretching spectral region of a solution of the all-*syn* tetrol in liquid deuterated chloroform is displayed in Fig. 2. For comparison, a complementary spectrum of the diastereomeric all-*anti* tetrol is also shown. The OH-stretching resonance of the all-*syn* diastereomer is qualitatively very similar to the OH-stretching resonance of monodeuterated water dissolved in heavy water.[22] It is centered at 3390 cm^{-1}, *i.e.* strongly red-shifted with respect to the OH-stretching resonance of monomeric alcohols in non-polar solutions.[23] It is furthermore very broad (full width at half maximum, FWHM $\approx$ 185 cm^{-1}) and has nearly a Gaussian shape. All these features unambiguously support the existence of intramolecular hydrogen-bonds as expected and theoretically predicted for this diastereomer. Hydrogen-bonds are broken only very occasionally as evidenced by the very weak absorption band centered at 3615 cm^{-1} that is reminiscent of dangling (or "free") hydroxyl groups primarily interacting with the non-polar solvent.

In contrast, the OH-resonance of the all-*anti* diastereomer qualitatively resembles a spectrum of alcohol oligomers in nonpolar solvents.[24–27] Firstly, a broad band peaking at 3470 cm^{-1} and having a width of 170 cm^{-1} (FWHM) indicates that despite the unfavorable stereochemistry, hydrogen-bonding can still occur. Secondly, this feature is considerably blue-shifted with respect to its all-*syn* counterpart thereby highlighting that the hydrogen-bonds in this system are much weaker as compared to those of the diastereomer. Thirdly, its absorption cross section is only half as large as that of its all-*syn* counterpart and its spectral shape is also markedly different. An extended tail to lower frequencies makes the line shape appear highly asymmetric. Taken together, all these findings hint at significantly different line broadening mechanisms, rates, and/or strengths that shape the OH-stretching resonances of these diastereomeric polyols. Finally, the rather narrow high-frequency band at 3620 cm^{-1} indicative of dangling (or free) hydroxyls has gained at the expense of the broad band from hydrogen-bonded OH. Obviously and because of their weaker character, the hydrogen-bonds can break much more frequently in the all-*anti* tetrol as compared to those of the all-*syn* system.

Because of the unfavorable stereochemical orientation of the hydroxyls along the hydrocarbon backbone (see Fig. 1) one might be tempted to conclude, that the broad OH-resonance of the all-*anti* polyol is brought about by intermolecular rather than intramolecular hydrogen-bonds. However, the formation of dimers and oligomers should facilitate the formation of even shorter and stronger hydrogen-bonds, which in turn should be reflected in a red-shift of the broad OH-resonance of the all-*anti* tetrol relative to its all-*syn* counterpart. Furthermore, intermolecular hydrogen-bonding with formation of higher aggregates should depend on the concentration.

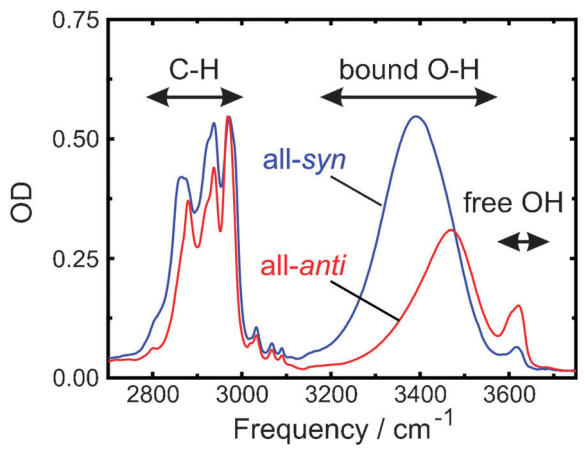

Fig. 2 Linear infrared absorption spectrum in the CH/OH stretching regions of the all-*syn* and all-*anti* tetrol in liquid $CDCl_3$ solution.

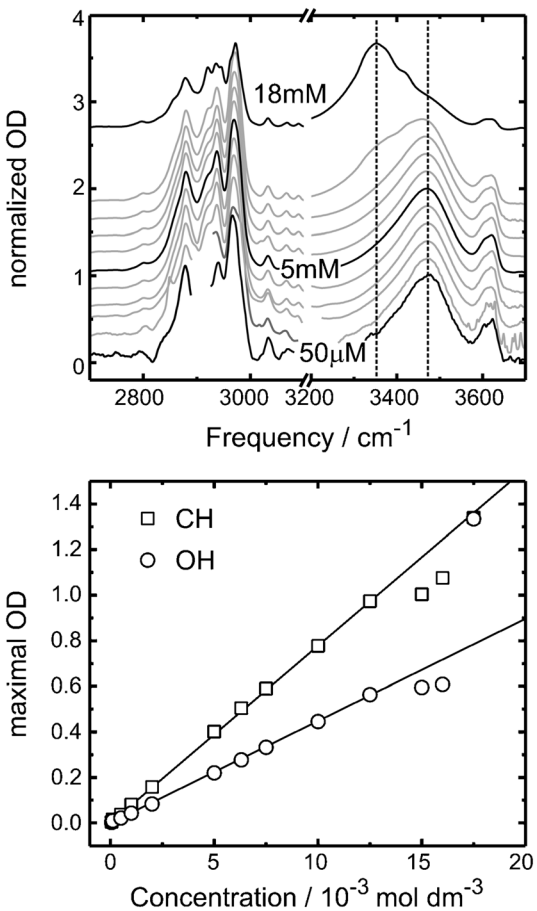

Fig. 3 Top: FTIR spectra in the OH-stretching region of the all-*anti* tetrol at solute concentrations of 0.05, 0.1, 0.5, 1.0, 2.0, 5.0, 7.5, 10, 12.5, 15, and 18 mM (from bottom to top). The spectra have been incrementally shifted along the ordinate for clarity. A solvent overtone precludes the reliable measurement of a solute optical density around 2900 cm^{-1} for very high dilutions. Bottom: Maximal optical densities in the OH (circles) and CH (squares) stretching region as a function of the molar solute concentration.

Fig. 3 displays a series of FTIR-spectra in the OH-stretching spectral region for various concentrations of the all-*anti* tetrol. It can be seen that the shape of the OH-resonance remains stable for concentrations up to about 13 mM. In addition, the maximal OH-stretching absorbance scales strictly linearly with the molar solute concentration from about 10 μM (our detection limit) up to 13 mM. Only for concentrations in excess 18 mM, the broad OH-resonance abruptly shifts by more than 100 cm^{-1} to lower frequencies and finds itself even red-shifted compared to the OH-band of the all-*syn* resonance. This sudden change of the FTIR spectrum clearly marks the onset of the formation of aggregates whose intermolecular H-bonds are even stronger that those of the all-*syn* tetrol. A further increase of the solute concentration eventually leads to precipitation. In this study, we worked at concentrations of 6 mM, *i.e.* well below the onset of aggregation. We therefore emphasize that regardless of the stereochemistry the hydrogen-bonds in our systems are fully intramolecular in nature. The existence of intramolecular hydrogen-bonds and in particular, the surprising formation of intramolecular H-bonds in the all-*anti* tetrol, is further fully corroborated by theoretical calculations of its geometrical structure based on density functional theory (see ref. 18).

To obtain more insight into the line broadening dynamics and the mechanism of vibrational relaxation, 2DIR spectroscopic experiments were carried out. Contour diagrams of 2DIR hole-burning spectra are reproduced in Fig. 4 for the two diastereomeric tetrols at a very early pump–probe (or waiting) delay of 500 fs. 2DIR spectra record the pump-induced (*i.e.* differential) optical density, $\Delta OD(\nu_{probe}, \nu_{probe}, t_W)$ as a function of the probe frequency, ν_{probe}, and the pump-center frequency, ν_{probe}, for a given pump–probe time delay, t_W. The spectra are composed of the expected ground state bleach/excited state stimulated emission signals (solid contours) and the anharmonically shifted excited-state absorption (dashed contours).

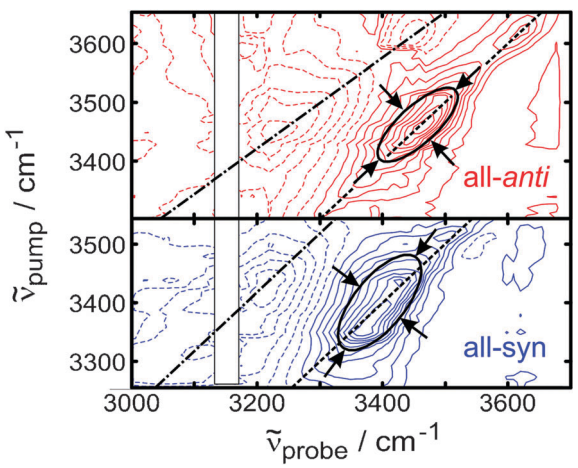

Fig. 4 2DIR spectrum of all-*anti* (top) and all-*syn* tetrol (bottom) dissolved in liquid $CDCl_3$ solution. The data were recorded for a waiting delay of 500 fs. The dashed lines correspond to the diagonal. The ellipses represent fits to the 50%-contours of the ground-state bleach/stimulated emission signals. The dotted-dashed lines emphasize the tilt of the excited-state absorption. The principal axes of the ellipses are indicated by the arrows.

The following observations can be made in the bleaching/emission region: firstly, both 2DIR spectra are elongated primarily along the diagonal indicating substantial inhomogeneous broadening of both H-bonded and free OH-stretching vibrations. Secondly, the spectral holes burnt into the H-bonded all-*anti* OH-resonance are significantly narrower than those burnt in the all-*syn* OH-resonance. This can be emphasized by fitting an ellipse to the contour representing a relative signal amplitude of 50% of the maximum bleach and calculating the ratio of the minor-to-major semi-axis (for details regarding the appropriateness of an ellipse to represent the 2DIR contours see ref. 28). Whereas for the all-*anti* tetrol, this ratio is ~3.9, a value of only ~1.5 is found for the all-*syn* tetrol. In addition, while for the former the ellipse is perfectly aligned along the diagonal, it is slightly tilted away toward the vertical for the latter. Both observations indicate that the degree of homogeneous broadening is much higher[28,29] for the all-*syn* tetrol.

Focusing now on the excited state absorption region of the 2DIR spectra, the following additional features can be noted: firstly, a narrow probe frequency interval (ranging from 3175 to 3200 cm^{-1}) is perturbed by the linear absorption of the $\nu_1 + \nu_4$ solvent combination band, which prohibits the measurement of reliable differential optical densities at early waiting delays. For this reason, this spectral window is disregarded for the moment. Secondly, despite the solvent artifact, an anharmonic shift—as measured by the frequency offset between the ground state bleach (solid contours) and the excited state absorption (dashed contours)—can be observed for the all-*anti* tetrol that increases with decreasing pump center frequency. At a first glance, this finding can be understood in terms of the conventional notion that the resonance frequency of the OH-oscillator gradually shifts to lower frequencies with increasing strength of the hydrogen bond to which it is coupled.[22,30] Consequently, the anharmonicity increases with increasing strength of the H-bond. Provided the resonance is at least partially inhomogeneously broadened, this would in turn result in a hyper-diagonal tilt of the 2DIR excited-state absorption line shape as is indeed observed for the all-*anti* tetrol (see dashed contours and dotted-dashed lines). Interestingly, such a hyper-diagonal tilt is not as clearly discernible for the all-*syn* tetrol, which—together with the findings from the 2DIR bleaching/emission line shape—hints again at different line broadening mechanisms for the two diastereomeric polyols (see below).

We now turn our attention to the lifetime of the OH-stretching vibrational excited state, $\tau(\nu_{pump})$, and its dependence on the excitation frequency. To this end, the decay of the anharmonically shifted transient absorption was calculated from the delay-dependent 2DIR spectrum as a function of the pump center frequency. To suppress temporal distortions of the signals such as non-exponential decays due to spectral diffusion dynamics, the excited state absorption was integrated over the probe frequency (within 50% of the maximum ΔOD). Within the signal-to-noise ratio and after the instantaneous coherent coupling/solvent response has subsided (*i.e.* for pump–probe delays larger than 700 fs), the resultant average transient absorption signals decay strictly mono-exponentially as shown in Fig. 5 for both diastereomers

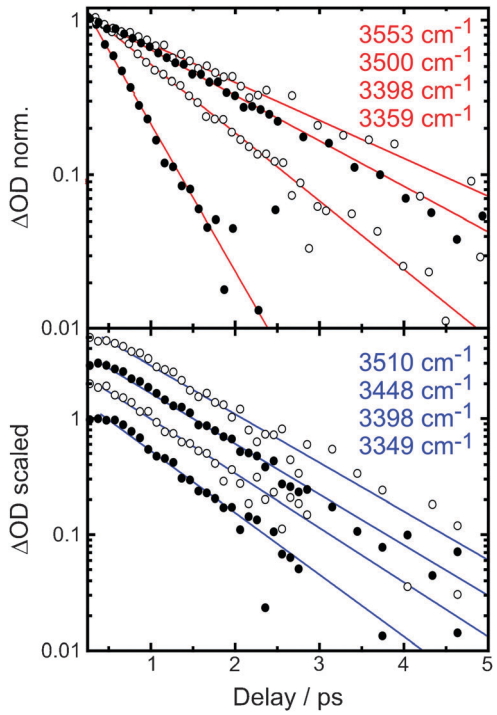

Fig. 5 Temporal decay of the probe-frequency integrated excited-state absorption of the all-*anti* (top) and all-*syn* (bottom) tetrol in liquid $CDCl_3$ solution for various pump center frequencies. The symbols are the experimental data and the solid lines are single-exponential fits.

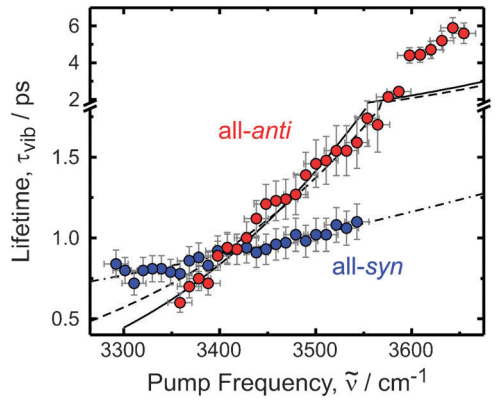

Fig. 6 Pump-frequency dependence of the OH-stretching vibrational lifetime determined from the probe-frequency integrated excited state absorption for the all-*anti* and the all-*syn* tetrol in liquid $CDCl_3$ solution. Note the break in the vertical axis. The solid curve corresponds to a fit using eqn (1) and a Gross phonon spectral density. The dashed and dotted-dashed curves are fits using the classical Landau-Teller expression (3). For details see text.

and for a few representative pump center frequencies distributed evenly across their respective OH-stretching region.

It can be seen that for the all-*anti* tetrol, the excited state absorption decays ever faster with gradually decreasing pump center frequency. In contrast, the decay of the signals obtained for the all-*syn* tetrol remains more or less unaffected by tuning the pump frequency. This strikingly different behavior of the OH-stretching excited state lifetime is summarized in Fig. 6. In particular across the H-bonded resonance of the all-*anti* species, the lifetime scales linearly with the pump center frequency decaying about 2.5 times faster when pumping at the red edge (τ = 0.7 ps around 3350 cm^{-1}) as compared to pumping at the blue edge (τ = 1.7 ps around 3550 cm^{-1}) of the broad OH-stretching absorption band. Furthermore, the lifetime of the dangling hydroxyls is approximately 5 ps, which is very similar to the OH-stretching lifetime of monomeric ethanol in carbon tetrachloride solution of 8 ps.[31] Finally, tuning the pump laser across the OH-stretching resonance of the all-*syn* tetrol yields a much weaker pump frequency dependence. One could even argue that within the error bars essentially the same lifetime of (0.95 ± 0.15) ps is measured.

How can this markedly different behavior of the excited state lifetime of the two diastereomeric polyols be rationalized? Apparently, for the all-*anti* stereochemical arrangement of hydroxyl groups, a narrowband pump pulse is able to selectively excite the OH-vibrators as if their resonance were inhomogeneously broadened. The mid-IR excitation selects from the total distribution of hydroxyl oscillators only the specific narrow sub-ensemble whose OH-stretching frequency—as determined by the instantaneous hydrogen-bond geometry—is matched to the center frequency of the driving field. Each sub-ensemble relaxes with its own unique OH-stretching vibrational lifetime whose magnitude is again defined by the structural details of its immediate environment including the hydrogen-bond geometry. In contrast, such a selective excitation can apparently not be performed as efficiently within the OH-stretching resonance of the all-*syn* tetrol.

Vibrational relaxation of liquid alcohols has been studied previously in great detail.[25,26,32–36] In particular, the intramolecular pathways for energy flow within n-alkanols were disentangled by IR-pump-Raman-probe spectroscopy[36] which indicates that an initial OH-stretching excitation decays primarily into a spatially nearby CH-stretching mode of the same molecule with the energy mismatch being compensated for by the low frequency phonon modes of the liquid. Such a mechanism is purely mechanical in nature and is dictated by cubic anharmonic couplings involving nuclear degrees of freedom of both the solute and the solvent. In principle, if the excited molecule were sufficiently large and flexible, the low frequency modes of the solute may also serve as a reservoir providing the phonon spectral density. In this case the relaxation becomes a purely intramolecular vibrational redistribution (IVR) process rather than a solvent assisted phenomenon. Furthermore, relaxations into the COH bending overtone or into any other overtone were discarded as possible pathways for efficient energy flow from the OH-stretch because they require quartic anharmonicities rather than cubic.[36,37] The COH bending overtone becomes important only for the subsequent relaxation of the CH-stretches because of their mutual near-resonance within the thermal energy.

In the case of our diastereomeric polyols, it might also very well be that a CH stretching mode serves as the doorway state through which the initial OH-stretching excitation relaxes. It is then the energy gap between the OH and CH stretching fundamentals that dictates the magnitude of the vibrational lifetime. An inspection of the linear absorption spectrum (Fig. 2) suggests that this energy gap can range somewhere

between 200 and 700 cm^{-1} depending upon the exact spectral location of the energy accepting CH-stretch. A tuning of the pump pulse across the entire OH-stretching band as was done here can easily account for a variation of the lifetime by a factor of two to three.

Following the work by Fayer and coworkers,[38] the rate constant for vibrational relaxation of a polyatomic solute embedded in a quantum reservoir is given by

$$k_{vib}(\tilde{\nu}_p) = [1 + n(\tilde{\nu}_a)][1 + n(\tilde{\nu}_p - \tilde{\nu}_a)]\rho(\tilde{\nu}_p - \tilde{\nu}_a) C(\tilde{\nu}_p - \tilde{\nu}_a) + n(\tilde{\nu}_a)[1 + n(\tilde{\nu}_p + \tilde{\nu}_a)] \rho(\tilde{\nu}_p + \tilde{\nu}_a) C(\tilde{\nu}_p + \tilde{\nu}_a) \quad (1)$$

provided the relaxation is governed by cubic anharmonicities. A high frequency intramolecular solute vibration (*i.e.* the relaxing solute mode pumped at the frequency, $\tilde{\nu}_p$, in wavenumber units) partitions into a solute mode (*i.e.* the acceptor mode at $\tilde{\nu}_a$) and a low-frequency phonon of the reservoir that is in resonance with the energy gap $\Delta\tilde{\nu} = \tilde{\nu}_p \pm \tilde{\nu}_a$. The spectral density of which is represented by $\rho(\tilde{\nu}_p \pm \tilde{\nu}_a)$ while $C(\tilde{\nu}_p \pm \tilde{\nu}_a)$ contains the anharmonic couplings. The quantity, $n(\tilde{\nu})$, corresponds to the Bose-Einstein occupation number at the frequency, $\tilde{\nu}$.

Using a frequency of the solute accepting mode around 2900 cm^{-1} consistent with the CH-stretching region and choosing a Gross line shape for the spectral density of the phonon band according to

$$\rho(\tilde{\nu}) = \frac{1}{2\pi}\frac{\gamma\tilde{\nu}}{(\tilde{\nu}_0^2 - \tilde{\nu}^2)^2 + \gamma^2\tilde{\nu}^2} \quad (2)$$

with $\tilde{\nu}_0$ = 50 cm^{-1} and γ = 200 cm^{-1}, the OH-stretching lifetime of the all-*anti* diastereomer can be modeled reasonably well (see solid curve in Fig. 6). The spectral density is significantly narrower than the far-infrared absorption spectrum of neat liquid chloroform[39] but tails off much slower to higher frequencies. The DFT calculations identify for the optimized 0 K structure of the all-*anti* diasteoreomer about 50 vibrational degrees of freedom with frequencies below 500 cm^{-1}. To what extent these intramolecular low-frequency backbone modes also contribute to the phonon spectral density is unclear.

The data can also be modeled similarly well using the classical Landau-Teller rate constant for an interaction-induced transition between two vibrational levels forming an energy gap, $\Delta\tilde{\nu}$, in wavenumber units[40]

$$k_{vib}(\Delta\tilde{\nu}) = 1/\tau_{vib}(\Delta\tilde{\nu}) = c\tilde{\nu}_0 \exp\{-3[T_{LT}(\Delta\tilde{\nu})/T]^{1/3}\}. \quad (3)$$

Here, $T_{LT} = 2\pi^4 c^2 \mu a^2 \Delta\tilde{\nu}^2/k_B$ is the characteristic Landau-Teller temperature, c is the speed of light, and k_B is Boltzmann's constant. Lacking detailed information regarding the interaction potential relevant to the energy relaxation, the product of the reduced mass, μ, and the square of the critical interaction distance, a^2, serves as a single fitting parameter as does the pre-factor, $\tilde{\nu}_0$. Employing a Landau-Teller temperature of 670 K at the maximum of the OH-stretching absorption band, *i.e.* at 3470 cm^{-1}, yields the dashed curve shown in Fig. 6. However, an unreasonably large pre-factor of 1400 cm^{-1} (*i.e.* similar to the COH-bending fundamental) is required, which questions the applicability of eqn (3) to the OH-stretching relaxation dynamics of the all-*anti* polyol.

Regardless of the applicability of either model, it seems quite reasonable that the pump-frequency dependence of the vibrational lifetime is a direct consequence of the selectivity of the pump pulse to selectively excite sub-ensembles from the inhomogeneously broadened resonance. Each sub-ensemble relaxes with its own unique lifetime that reflects the magnitude of the energy gap between the energy accepting solute vibration and the solute's OH-stretching fundamental.

The question remains as to why the vibrational lifetime of the all-*syn* tetrol is so insensitive to changes of the pump-frequency as compared to that of its all-*anti* counterpart. Notice that in Fig. 6 more or less the same pump frequency region was used for exciting the two diastereomeric polyols. Therefore, if both resonances were equally inhomogeneously broadened, the energy gap range that is effectively sampled by tuning the excitation pulse across the OH-stretching absorption band would essentially be the same for the two molecules. Whereas eqn (1) is unable to provide a satisfactory fit to the all-*syn* data, a good description is obtained from eqn (3) with a Landau-Teller temperature of 17 K at the maximum of the linear OH-stretching absorption (3390 cm^{-1}) and a pre-factor of 120 cm^{-1}. In contrast to the all-*anti* tetrol, these parameters are similar in magnitude to those for HOD in D_2O obtained in ref. 41 from the equivalent Schwarz-Slawsky-Herzfeld expression for the rate constant.[42]

Only two possibilities remain to rationalize the stark contrast between the two diastereomers. Either the phonon spectral densities of the baths are not the same or the mechanism for vibrational energy relaxation is markedly different.

Regarding the first possibility, we do not see at the moment any reason for a modification of the phonon spectral density when altering the stereochemical orientation of adjacent hydroxyl groups along the hydrocarbon backbone. This is because the infrared spectra in the CH-stretching region are almost identical (*cf.* Fig. 2) for both molecules. There is no significant infrared activity in the region between 1500 and 2800 cm^{-1} and from 1500 cm^{-1} down to about 1000 cm^{-1}, their spectra are again very similar. Our previous DFT calculations furthermore indicated that the low-frequency vibrational manifolds below 1000 cm^{-1} are similarly dense.[18] Finally, for both molecules the same solvent was used and the solvent contribution to the phonon spectral density should therefore also be the same. Therefore, we are led to the conclusion that the distinct pump-frequency dependence of their vibrational lifetimes is a direct consequence of the different character of the OH-stretching modes and the line-broadening dynamics these modes experience.

The DFT calculations reported earlier[18] have shown that at zero Kelvin the minimum energy structure of the all-*anti* tetrol features a highly strained hydrogen-bonded network whose OH-stretching modes are predominantly localized on the four hydroxyl groups. In contrast, the same DFT methodology reveals a minimum energy structure of the all-*syn* tetrol whose OH-groups are perfectly aligned to form an extended quasi-linear chain of hydrogen bonds. Adjacent OH-dipoles are aligned head-to-tail and almost perfectly parallel thereby

optimizing their mutual dipole–dipole interaction. The cooperative alignment of the hydroxyls and the stronger coupling among all the OH-vibrators as compared to the all-*anti* tetrol fully delocalizes the four local OH-stretching modes of the all-*syn* tetrol over its hydrogen-bonded chain, *i.e.* the four OH-stretching modes involve the collective motion of all hydroxyls and are therefore best described as normal modes at zero Kelvin.

The vibrational exciton model has been used successfully in the recent past to describe the linear and non-linear infrared spectroscopy as well as the line broadening dynamics in molecular systems exhibiting weakly coupled modes of predominantly local mode character.[43,44] An intriguing application of this model is the elucidation of the dynamical structure of polypeptides by exploiting the small interactions between their amide I (CO) vibrators.[20,45] Restricting ourselves for the moment to a discussion of the zero Kelvin DFT-optimized structures, the all-*anti* tetrol can be regarded to fall into this particular regime of weakly coupled local vibrators (giving rise to four local OH-stretches), while the all-*syn* tetrol is a representative of a molecular system featuring comparatively strongly coupled oscillators that give rise to delocalized collective vibrations[46–48] (here the four OH-normal modes). Formally, the all-*syn* polyols bear some structural resemblance to coupled electronic chromophores[49,50] (*e.g.* J-aggregates), where the electronic eigenstates are delocalized over a spatially extended stack of molecules that are held together by dipole–dipole interactions. In the all-*syn* tetrol at 0 K the vibrational eigenstates are delocalized over the extended chain of hydroxyl groups that are aligned in parallel by the very same type of through-space interaction. Just as in J-aggregates the parallel transition dipoles are oriented head-to-tail and the nearest neighbor coupling is negative.[49,50]

We can test the importance of transition dipole coupling for the zero-Kelvin structure of the all-*syn* system by comparing its normal modes obtained from the DFT calculation with predictions from a simple exciton model calculation. The four OH normal modes of the all-*syn* tetrol were located at 3404, 3459, 3487, and 3494 cm^{-1} with dipole strengths of 0.393, 0.206, 0.171, and 0.104 D. The transition dipole–dipole coupling elements can be calculated from the DFT-optimized structure according to

$$\beta_{ij} = \vec{\mu}_i \cdot \vec{\mu}_j |\vec{r}_{ij}|^{-3} - 3(\vec{r}_{ij} \cdot \vec{\mu}_i)(\vec{r}_{ij} \cdot \vec{\mu}_j)|\vec{r}_{ij}|^{-5}, \quad (5)$$

where $\vec{\mu}_i$ and $\vec{\mu}_j$ are the transition dipoles attributed to two local hydroxyl sites, i and j, while $\vec{r}_{ij}$ is the vector interconnecting them. Taking the local site transition dipoles to be oriented exactly along the four OH-bonds with a magnitude of 0.196 D,[51,52] the three nearest neighbor coupling constants are then directly found from eqn (5) and the structural data from ref. 18 to be $\beta_{i,i+1} = -16.3\ cm^{-1}$, $-15.8\ cm^{-1}$, and $-16.4\ cm^{-1}$. Likewise, the two couplings between next-nearest neighbors are identified as $\beta_{i,i+2} = -2.2\ cm^{-1}$ and $-2.0\ cm^{-1}$ while the second-next-nearest neighbor interaction is $\beta_{i,i+3} = -0.6\ cm^{-1}$. As pointed out above, all couplings are negative because of the nearly perfect parallel head-to-tail alignment of the four hydroxyls, whose bond dipoles are tilted away from the vectors interconnecting adjacent sites by no more than 30°. The relative orientation of the site dipoles is displayed in Fig. 7 from three different perspective angles.

To simplify the exciton model and to reduce the number of free-floating fitting parameters (*i.e.* the site energies), we assume that the hydroxyl oscillators terminating the hydrogen-bonded chain have the same frequency but different from those of the internal hydroxyls. Diagonalization of the constructed one-exciton Hamiltonian provides the set of four coupled eigenstates whose deviation from the four DFT-normal mode eigenstates was minimized to an agreement of better than $10^{-5}\ cm^{-1}$ by nonlinear least-squares fitting of the remaining three site energies. The resultant eigenvectors are then used to construct the excitonic transition dipoles from the set of four site transition dipoles. Their magnitude and their spatial orientation are compared in Fig. 7 with the results from the normal mode analysis. The agreement between the two types of dipoles is excellent. In addition, internal site frequencies of 3465 cm^{-1} and 3412 cm^{-1} are found, both of which are lower than the terminal site frequency (3483 cm^{-1}) as expected in such hydrogen-bonded chains. Indeed, the latter value coincides with the frequency reported for the terminal hydroxyl groups of alcohol oligomers in nonpolar solvents. The excellent agreement between the normal modes and the vibrational excitons indicates that *the predominant mechanism that couples the local hydroxyl oscillators in our linear chains of hydrogen bonds is indeed transition dipole interaction*. This is further substantiated by a Hessian reconstruction[53] performed directly on the DFT results using the magnitude of the hydrogen atom contribution to the normal modes to deduce the excitonic wavefunctions. This procedure reveals essentially the same results with similar site frequencies as those derived above.

So far we have only discussed the importance of transition dipole–dipole coupling for the all-*syn* structure at zero Kelvin. Previous Langevin molecular dynamics simulations were aimed at studying the influence of a condensed phase environment at finite temperature on the molecular structure of these polyols.[18] For the all-*anti* tetrol at room temperature, it was observed that H-bonds can break and reform multiple times within a period as short as 1 ps while such large amplitude hydrogen-bond dynamics can occur only sporadically in the all-*syn* diastereomer. This difference is also manifest by the remarkably distinct stationary FTIR spectra as shown in Fig. 2. Hence, the all-*syn* tetrol features a linear hydrogen-bond network that is stable for tens of picoseconds even at room temperature. Nevertheless, rapid small scale structural fluctuations of the hydrogen-bond distances and angles can still occur, which inevitably introduces dynamic diagonal and off-diagonal disorder into the one-exciton Hamiltonian.

To estimate the homogeneous contribution of such structural fluctuations to the overall absorption line width associated with the OH-stretching resonance, cuts through the ground-state bleach/stimulated emission component of the 2DIR spectra along their anti-diagonal were calculated for both diastereomers. The experimental data together with fits to a Lorentzian line shape are displayed in Fig. 8. It is clearly visible that the all-*syn* species exhibits a significantly larger

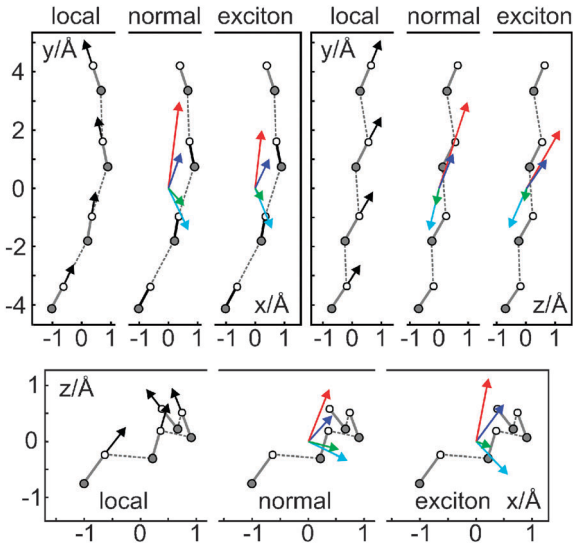

Fig. 7 View of the spatial arrangement of the four hydroxyl oscillators in the all-*syn* tetrol from three different perspectives. The gray and white circles represent the oxygen and hydrogen atoms. The gray solid lines are the OH-bonds and the gray dashed lines represent the hydrogen-bonds. The local site transition dipoles are indicated by the arrows as are the normal mode transition dipoles and those of the OH-stretching excitons.

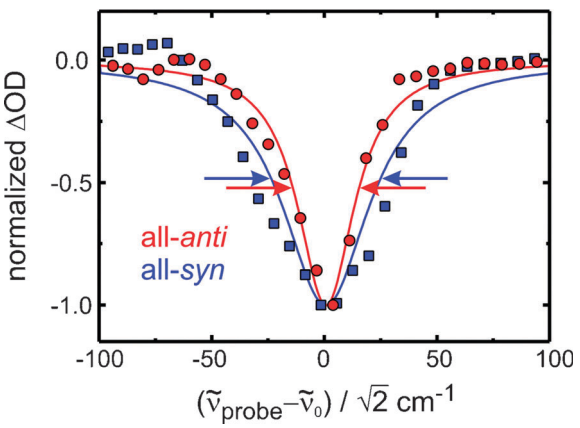

Fig. 8 Cuts through the 2DIR spectra along the anti-diagonal for the all-*anti* (circles) and all-*syn* (squares) tetrol in liquid $CDCl_3$ solution. The symbols correspond to the experimental data whereas the solid curves are fits to Lorentzian spectral line shapes. The arrows emphasize the full anti-diagonal widths at half maximum.

homogeneous linewidth (47 cm^{-1}) as compared to the all-*anti* diastereomer (28 cm^{-1}).

At a first glance, a larger homogeneous linewidth for the all-*syn* tetrol appears to be in contradiction with the Langevin simulations, in which ultrafast hydrogen-bond breakage and formation became apparent only for the all-*anti* tetrol. The different homogeneous linewidths can neither be rationalized by vibrational anharmonicity effects as the 2DIR spectra reveal anharmonic shifts between the ground state bleach and the excited state absorption that are very similar for both systems (*cf.* Fig. 4). The larger homogeneous linewidth indicates most likely that at room temperature the couplings among the OH-oscillators is still significantly larger for the all-*syn* tetrol as compared to those of the all-*anti* diastereomer. Calculating the inter-hydroxylic couplings for the DFT-optimized structure of the all-*anti* tetrol using eqn (5) and the same dipole strength as above we find that at zero Kelvin the values for $\beta_{i,i+1}$ are only about 20% smaller than for the all-*syn* tetrol. This difference is too small to fully account for the different homogeneous linewidths of the two systems. However, the OH transition dipoles of the all-*syn* tetrol are likely to be further enhanced because of the nearly perfect alignment of its OH-groups and the cooperativity of the hydrogen bonds: Such a non-Condon effect is well documented for the OH stretching vibrations of liquid water, where the transition dipole is also larger for the hydroxyl oscillators involved in the strongest hydrogen bonds.[54] Indeed, the peak absorptions originating from the hydrogen-bonded OH-stretching oscillators of the two diastereomeric tetrols differ by roughly a factor of two. Therefore, the magnitude of the couplings among the four OH-oscillators is expected to be much larger for the all-*syn* diastereomer, thereby quite naturally rationalizing its larger homogeneous linewidth in comparison to the all-*anti* diastereomer.

A comparison of the homogenous linewidths with the apparent absorption bandwidths crudely suggests an inhomogeneous broadening of somewhere between 100 and 140 cm^{-1} for both systems. From these numbers one has to conclude that at room temperature the vibrational excitations are mostly localized on the individual hydroxyl groups of both diastereomers. However, it is the different magnitude of the inter-hydroxylic coupling that distinguishes the two diastereomeric tetrols from each other. In the absence of vibrational energy relaxation to modes other than OH-stretch, an initially deposited OH-stretching quantum will ultimately hop from one local hydroxyl oscillator to another in a random fashion. However, the hopping rate will depend on the strength of the interaction between pairs of OH-groups.

In the all-*anti* tetrol, where the couplings are rather weak and the structure is very irregular, this OH-stretching excitation will continue to reside on the initially excited oscillator for a much longer time as compared to the all-*syn* tetrol where the structure is more robust and the couplings are stronger. Consequently, vibrational relaxation from the collection of all-*anti* oriented hydroxyls will occur primarily from the very same OH-vibrator pumped at zero time delay. As mentioned above, the relaxation rate is governed by the actual energy gap between this initially excited oscillator and the accepting CH-stretching mode. The pump-frequency dependence of the relaxation rate of the all-*anti* diastereomer is thus a direct consequence of the inhomogeneous broadening of the OH-resonance in combination with the relatively long residence time of the vibrational excitation on the local hydroxyl oscillator selected by the pump.

Quite in contrast, an OH-stretching excitation initially deposited into a given local hydroxyl oscillator of the all-*syn* tetrol will randomly redistribute among all the other OH-groups prior to complete vibrational relaxation into the CH-stretching manifold. The primary redistribution essentially establishes a quasi-thermalization of the excess energy over the v = 1 OH-stretching manifold and consequently, a vibrational

relaxation rate is experimentally measured that corresponds to a "thermal average" over the four OH-to-CH-stretching transition rates. Since this OH-stretching randomization will occur regardless of the precise spectral location of the pump pulse, a pump-frequency independent rate as seen in Fig. 6 should be obtained. In other words, for the process of vibrational energy relaxation, the hydroxyl stretching redistribution causes effectively an ultrafast loss of memory regarding the frequency of initial excitation. A minor residual dependence of the vibrational relaxation rate on the pump center frequency might arise because a strict time scale separation between OH-randomization and OH-to-CH energy transfer as sketched above may not be fully warranted.

Conclusions

In summary, we have measured the OH-stretching vibrational lifetime of two diastereomeric poly-alcohols featuring a sequence of four hydroxyl oscillators. Depending upon the relative stereochemistry of the OH groups, the polyalcohol can either support the formation of a quasi-linear chain of hydrogen bonds that is stable over tens of picoseconds (all-*syn*) or it can display ultra-rapid dynamics of H-bond breakage and formation (all-*anti*). In the latter case, the OH-stretching vibrational lifetime is a very strong function of the excitation center frequency. In parallel, narrow spectral holes are seen along the anti-diagonal of the early-time 2DIR spectrum. Apparently, the pump pulse is able to selectively excite from the inhomogeneously broadened OH-stretching resonance a specific sub-ensemble that relaxes with its own unique vibrational lifetime as defined by the sub-ensemble's instantaneous hydrogen-bonding environment. The H-bonding configuration in turn determines the frequency of the hydroxyl stretching fundamental and the magnitude of the energy gap to the accepting modes. It is the sensitivity of this energy gap to the local structure together with the localized nature of an OH-stretching excitation among an inhomogeneously broadened resonance that is responsible for the pronounced frequency dependence of the vibrational lifetime of the all-*anti* polyol.

In stark contrast, the vibrational lifetime of the all-*syn* polyol contains only a very weak dependence on the excitation frequency. In parallel, spectral anti-diagonal holes seen in the 2DIR spectrum are considerably broader indicative of a shorter homogeneous dephasing time as compared to the diastereomeric polyol. We interpret these findings by invoking stronger transition-dipole interactions among the set of four hydroxyl oscillators as compared to the all-*anti* tetrol. As a consequence, an initial OH-stretching excitation will randomize along the hydrogen-bonded chain much more rapidly as compared to the more disordered diastereomer. In the limiting case where this redistribution within the $v = 1$ OH-stretching manifold is completed prior to vibrational energy relaxation, the decay of the transient absorption essentially reports a vibrational lifetime that is averaged over the set of four OH-stretching modes regardless of the frequency of excitation.

We are currently working on analyzing the dependence of the vibrational lifetime on the number of hydroxyls attached to the hydrocarbon backbone. This will allow us to explore in particular any size effects related to the linear spectroscopy and the vibrational relaxation dynamics of the OH-stretching vibrational excitons. Furthermore, a detailed report and an in depth analysis of the temporal evolution of the 2DIR spectra of the diastereomeric polyols are underway.

Acknowledgements

Financial support by the Deutsche Forschungsgemeinschaft through the Collaborative Research Centers, SFB 624 "-Functional Chemical Templates" and SFB 813 "Chemistry at Spin Centers" is gratefully acknowledged. We are indebted to Dirk Schwarzer and his coworkers for conducting the chemical synthesis of the polyols and to Frank Wennmohs for continued support in electronic structure calculations.

References

1 P. Schuster, G. Zundel and C. Sandorfy, *The hydrogen bond: Recent Developments*, North Holland, Amsterdam, 1976.
2 G. A. Jeffrey, *An intrduction to hydrogen bonding*, Oxford University Press, New York, 1997.
3 *Ultrafast Hydrogen Bonding Dynamics and Proton Transfer Processes in the Condensed Phase*, ed. T. Elsaesser and H. J. Bakker, Kluwer Academic Publisher, Dordrecht, 2003.
4 E. T. J. Nibbering and T. Elsaesser, *Chem. Rev.*, 2004, **104**, 1887–1914.
5 S. Woutersen and H. J. Bakker, *Nature*, 1999, **402**, 507–509.
6 S. Woutersen and H. J. Bakker, *Comm. Mod. Phys.*, 2000, **2**, D99–D112.
7 M. F. Kropman, H. K. Nienhuys, S. Woutersen and H. J. Bakker, *J. Phys. Chem.*, 2001, **105**, 4622–4626.
8 D. Schwarzer, J. Lindner and P. Vöhringer, *J. Phys. Chem. A*, 2006, **110**, 2858–2867.
9 T. Schäfer, J. Lindner, P. Vöhringer and D. Schwarzer, *J. Chem. Phys.*, 2009, **130**, 224502–224508.
10 J. Lindner, D. Cringus, M. S. Pshenichnikov and P. Vöhringer, *Chem. Phys.*, 2007, **341**, 326–335.
11 N. Huse, S. Ashihara, E. T. J. Nibbering and T. Elsaesser, *Chem. Phys. Lett.*, 2005, **404**, 389–393.
12 S. Ashihara, N. Huse, A. Espagne, E. T. J. Nibbering and T. Elsaesser, *J. Phys. Chem. A*, 2007, **111**, 743–746.
13 C. J. Fecko, J. D. Eaves, J. J. Loparo, A. Tokmakoff and P. L. Geissler, *Science*, 2003, **301**, 1698–1702.
14 J. J. Loparo, S. T. Roberts and A. Tokmakoff, *J. Chem. Phys.*, 2006, **125**, 194521.
15 J. B. Asbury, T. Steinel, C. Stromberg, S. A. Corcelli, C. P. Lawrence, J. L. Skinner and M. D. Fayer, *J. Phys. Chem. A*, 2003, **108**, 1107–1119.
16 J. R. Schmidt, S. T. Roberts, J. J. Loparo, A. Tokmakoff, M. D. Fayer and J. L. Skinner, *Chem. Phys.*, 2007, **341**, 143–157.
17 S. T. Roberts, K. Ramasesha and A. Tokmakoff, *Acc. Chem. Res.*, 2009, **42**, 1239–1249.
18 J. Seehusen, D. Schwarzer, J. Lindner and P. Vöhringer, *Phys. Chem. Chem. Phys.*, 2009, **11**, 8484–8495.
19 I. Paterson and J. P. Scott, *J. Chem. Soc., Perkin Trans. 1*, 1999, 1003–1014.
20 P. Hamm, M. Lim and R. M. Hochstrasser, *J. Phys. Chem. B*, 1998, **102**, 6123.
21 I. Paterson and J. P. Scott, *Tetrahedron Lett.*, 1997, **38**, 7445–7448.
22 A. Kandratsenka, D. Schwarzer and P. Vöhringer, *J. Chem. Phys.*, 2008, **128**, 244510–244516.
23 R. Laenen and C. Rauscher, *J. Mol. Struct.*, 1998, **448**, 115–119.
24 R. Laenen and C. Rauscher, *J. Chem. Phys.*, 1997, **107**, 9759–9763.
25 R. Laenen and C. Rauscher, *J. Chem. Phys.*, 1997, **106**, 8974–8980.
26 S. Woutersen, U. Emmerichs and H. J. Bakker, *J. Chem. Phys.*, 1997, **107**, 1483–1490.
27 O. Kristiansson, *J. Mol. Struct.*, 1999, **477**, 105–111.
28 K. Lazonder, M. S. Pshenichnikov and D. A. Wiersma, *Opt. Lett.*, 2006, **31**, 3354–3356.

29 D. Kraemer, M. L. Cowan, A. Paarmann, N. Huse, E. T. J. Nibbering, T. Elsaesser and R. J. D. Miller, *Proc. Natl. Acad. Sci. U. S. A.*, 2008, **105**, 437–442.
30 A. Novak, *Structure and Bonding*, 1974, **18**, 177–216.
31 R. Laenen and C. Rauscher, *Chem. Phys. Lett.*, 1997, **274**, 63–70.
32 R. Laenen, C. Rauscher and A. Laubereau, *J. Phys. Chem. A*, 1997, **101**, 3201–3206.
33 K. J. Gaffney, P. H. Davis, I. R. Piletic, N. E. Levinger and M. A. Fayer, *J. Phys. Chem. A*, 2002, **106**, 12012–12023.
34 K. J. Gaffney, I. R. Piletic and M. D. Fayer, *J. Phys. Chem. A*, 2002, **106**, 9428–9435.
35 L. K. Iwaki and D. D. Dlott, *Chem. Phys. Lett.*, 2000, **321**, 419–425.
36 Z. Wang, A. Pakoulev and D. D. Dlott, *Science*, 2002, **296**, 2201–2203.
37 L. K. Iwaki and D. D. Dlott, *J. Phys. Chem. A*, 2000, **104**, 9101–9112.
38 V. M. Kenkre, A. Tokmakoff and M. D. Fayer, *J. Chem. Phys.*, 1994, **101**, 10618–10629.
39 J. T. Kindt and C. A. Schmuttenmaer, *J. Chem. Phys.*, 1997, **106**, 4389–4400.
40 E. E. Nikitin and J. Troe, *Phys. Chem. Chem. Phys.*, 2008, **10**, 1483–1501.
41 G. M. Gale, G. Gallot and N. Lascoux, *Chem. Phys. Lett.*, 1999, **311**, 123–125.
42 R. N. Schwartz, Z. I. Slawsky and K. F. Herzfeld, *J. Chem. Phys.*, 1952, **20**, 1591–1599.
43 S. Mukamel and D. Abramavicius, *Chem. Rev.*, 2004, **104**, 2073–2098.
44 A. Paarmann, T. Hayashi, S. Mukamel and R. J. D. Miller, *J. Chem. Phys.*, 2008, **128**, 191103–191105.
45 N. Demirdoven, C. M. Cheatum, H. S. Chung, M. Khalil, J. Knoester and A. Tokmakoff, *J. Am. Chem. Soc.*, 2004, **126**, 7981.
46 P. W. Anderson, *J. Phys. Soc. Jpn.*, 1954, **9**, 316–339.
47 B. M. Auer and J. L. Skinner, *J. Chem. Phys.*, 2008, **128**, 224511–224512.
48 T. L. C. Jansen, B. M. Auer, M. Yang and J. L. Skinner, *J. Chem. Phys.*, 2010, **132**, 224503.
49 E. E. Jelley, *Nature*, 1936, **138**, 1009–1010.
50 G. Scheibe, *Angew. Chem.*, 1937, **50**, 51.
51 The magnitude of the site transition dipole (0.196 D) was taken as the average of the dipoles obtained from the DFT calculation on the all-anti tetrol, which features OH-stretching modes that are predominantly local modes. For reference, the transition dipole of the OH-stretch in neat liquid methanol was determined to be 0.264 D.
52 J. E. Bertie and S. L. L. Zhang, *J. Mol. Struct.*, 1997, **413**, 333–363.
53 S. Ham, S. Cha, J. H. Choi and M. Cho, *J. Chem. Phys.*, 2003, **119**, 1451–1461.
54 J. R. Schmidt, S. A. Corcelli and J. L. Skinner, *J. Chem. Phys.*, 2005, **123**, 044513.

